

Magnetism of epitaxial Tb films on W(110) studied by spin-polarized low-energy electron microscopy

J.E. Prieto*

*Centro de Microanálisis de Materiales, Dpto. de Física de la Materia Condensada,
IFIMAC and Instituto "Nicolás Cabrera," Universidad Autónoma de Madrid, E-28049 Madrid, Spain*

Gong Chen (陈宫) and A.K. Schmid

Lawrence Berkeley National Laboratory, Berkeley, California 94720, USA

J. de la Figuera

Instituto de Química Física "Rocasolano," CSIC, Madrid 28006, Spain

(Dated: March 6, 2024)

Thin epitaxial films of Tb metal were grown on a clean W(110) substrate in ultra-high vacuum and studied in-situ by low-energy electron microscopy. Annealed films present magnetic contrast in spin-polarized low-energy electron microscopy. The energy dependence of the electron reflectivity was determined and a maximum value of its spin asymmetry of about 1% was measured. The magnetization direction of the Tb films is in-plane. Upon raising the temperature, no change in the domain distribution is observed, while the asymmetry in the electron reflectivity decreases when approaching the critical temperature, following a power law $\sim (1 - T/T_C)^\beta$ with a critical exponent β of 0.39.

PACS numbers: 68.37.Nq, 75.70.Kw, 68.55.J-, 75.70.Ak

I. INTRODUCTION

The hardest magnetic materials known to date¹ are inter-metallic systems containing magnetic rare earths (RE) alloyed with 3d transition metals (TM), as in Co-Sm and Nd-Fe-B. In these compounds, the high magnetic anisotropies are induced by the RE ions, while the characteristic high ordering temperatures of the ferromagnetic TMs are retained². These magnetic materials are widely used in applications that require strong permanent magnetic fields, raising concerns about the availability of the required rare earths. In consequence, lanthanides have been considered as model systems for the effect of increasing the anisotropy of TMs^{3,4}. Lanthanide metals themselves form a class of magnetic materials with rather different magnetic characteristics as compared to TMs. The negligible overlap between the partially filled electronic $4f$ shells of neighboring atoms in lanthanides leads to strongly localized magnetic moments, which in general contain both an orbital and a spin part. The localized character of the $4f$ moments is also responsible for the negligibly small direct exchange interaction between lanthanide ions. Instead, they couple only indirectly through the valence-band electrons of the metal⁵ (RKKY interaction), leading to ordering temperatures which are typically below room temperature (RT). The induced valence-band polarization gives only a minor contribution to the magnetization⁶, in contrast to the predominantly itinerant moments of ferromagnetic TMs.

In particular, heavy rare-earth metals are interesting magnetic materials due to their different magnetic properties despite their similar crystalline and electronic structures. For example, Gd and Tb crystallize in the hexagonal close-packed structure with lattice parameters that differ by less than 2%. On the one hand, the spherical charge distribution of the half-filled $4f$ shell of Gd leads to only a small magnetocrystalline

anisotropy and hence to small coercive fields in epitaxial films of good crystalline quality. On the other hand, Tb shows a large magnetic anisotropy⁷ due to its non-spherical $4f$ -charge distribution caused by a large atomic orbital momentum ($L=3$) which forces the magnetization to be in the basal plane. The easy axis is $\langle 10\bar{1}0 \rangle$ at all temperatures. Tb is ferromagnetic below 221 K, while between 221 K and 229 K it presents an helical magnetic structure than can be driven to a ferromagnetic arrangement by applied magnetic fields⁸. The magnetic moment per atom is $9.34 \mu_B$ with only a small contribution (of the order of the fractional part, $0.34 \mu_B$) from itinerant electrons.

Pure lanthanide-metal thin films have not been so widely studied as compared with TM films, in part due to their high chemical reactivity. For example just one study reported the distribution of magnetic domains in Dy films, by means of spin-polarized scanning tunneling microscopy⁹. In particular, no results of low-energy electron microscopy (LEEM) on lanthanide films have been reported to date. LEEM is a powerful technique allowing to visualize the surface morphology with a resolution of several nanometers and to study surface processes (e.g. crystal growth) in real time¹⁰. If spin-polarized electrons are used as an illumination source (spin-polarized LEEM or SPLEEM¹¹), the magnetic domain distribution of the films can be imaged in real space by using exchange scattering. In this work, we prepared epitaxial films of Tb on W(110) and imaged their magnetic domains by means of SPLEEM.

II. EXPERIMENTAL

Epitaxial Tb metal films of thicknesses of up to about 20 ML were prepared in situ by vapor deposition in ultra-high vacuum on a single-crystalline W(110) substrate, which

had been cleaned previously by cycles of oxygen exposure and high-temperature flashing, following a procedure known to produce clean and ordered W(110) surfaces well suited for subsequent growth of metallic films¹²⁻¹⁴. A high-purity Tb rod heated by electron bombardment was used as evaporation source. Deposition rates were of the order of 0.1 nm per minute. The base pressure in the chamber was in the 10^{-11} Torr range and rose to about 7×10^{-10} Torr when evaporating Tb. The vacuum chamber was equipped with a conventional electron optics for performing low-energy electron diffraction and a cylindrical mirror analyzer for recording Auger electron spectra. The sample temperature was measured by means of a WRe thermocouple attached to a molybdenum plate on which the W(110) crystal rests. The absolute error of our temperature measurement arises from the lack of a cold reference, from additional junctions of different materials and from the contact point of the WRe thermocouple with a washer underneath the sample. It can be as high as 10-20 K, as determined by comparing selected transitions observed both with the WRe thermocouple and a Pt1000 resistor. However the relative error is much smaller, in particular in our measurements as a function of the temperature, where no use was made of the sample heating filament so all the sample holder block was in thermal equilibrium with the cooling stage.

Spin-polarized LEEM measurements were performed in a low-energy electron microscope equipped with a spin-polarized electron source and a spin manipulator to adjust the spin direction of the electron beam with respect to the sample surface. Magnetic imaging is achieved in SPLEEM by representing the difference between LEEM images obtained with electron beams of opposite spin polarizations and normalizing by the sum. The intensity in the resulting SPLEEM images depends on the projection of the local surface magnetization onto the direction of spin polarization of the electron beam. As the electron-beam spin polarization can be changed with respect to the sample, the magnetization vector can be determined in real space with nanometer resolution¹⁵. More details on both the instrument¹⁶, the spin-polarization control method¹⁷, or the vector magnetometric application of SPLEEM^{15,18} can be found in the literature. The electron beam energy is referred to zero energy which corresponds to the sample and the cathode at the same potential.

III. RESULTS AND DISCUSSION

A typical image of the clean W(110) surface prior to deposition shows step bunches, as can be seen in Fig. 1a. Immediately after starting the deposition of Tb at room temperature, the step contrast is lost and a strong decrease of the reflected electron intensity is detected. In LEEM this is typically due to the nucleation of islands with sizes below the resolution limit of the microscope (typically ~ 30 nm). Continuing the deposition, the reflected intensity reaches a minimum. After the minimum (at about 1 minute of evaporation time), the step bunches begin to be weakly detected again, and the averaged reflected intensity recovers partially and then oscillates with a small amplitude, as shown in Fig. 2. Up to 4 max-

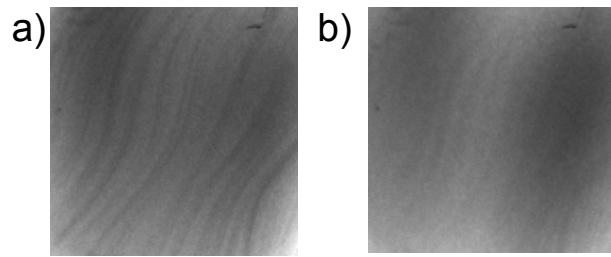


FIG. 1. (a) LEEM image of the clean W(110) surface prior to deposition. The electron energy is 5.4 eV and the field of view is $7.5 \mu\text{m}$. (b) LEEM image of the as-grown 4 ML Tb/W(110) film. The electron energy is 6.2 eV and the field of view is $7.5 \mu\text{m}$.

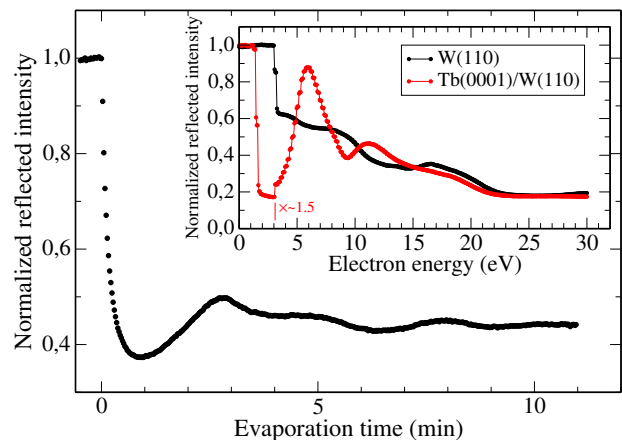


FIG. 2. (color online) Electron reflectivity at an electron energy of 5.4 eV as a function of the Tb evaporation time on the clean W(110) surface, normalized to the value prior to deposition start. Inset: Reflected electron intensity as a function of energy for both the 4 ML Tb(0001)/W(110) film and the substrate W(110). Intensities have been normalized to their respective maximum values and there is an increase in gain by a factor of about 1.5 due to a change in the detector settings in the curve for the film at an energy of about 3 eV.

ima in the intensity can be seen for a deposition time of about 11 min. A ratio of the intensities of the Auger electron transitions $\text{Tb}_{146 \text{ eV}}$ and $\text{W}_{179 \text{ eV}}$ of 9.9 was determined experimentally. Using the values for the inelastic electron mean free paths from Seah and Dench¹⁹ and tabulated sensitivity factors²⁰, a coverage of about 4.5 ML can be deduced, so that the observed intensity maxima can be attributed to the completion of successive monolayers.

The inset of Fig. 2 shows the reflected electron intensity as a function of the electron energy, both for the clean W(110) surface and for the 4 monolayer (ML) Tb/W(110) film. Intensities have been normalized to their respective values at zero energy. The initial drop of the reflected intensity marks the transition from mirror mode, where the electron energy lies below the work function of the surface, to regular diffraction imaging¹⁰. The decrease in the transition energies indicates that the Tb film has a work function which is lower by 1.7 eV than the bare W(110) surface, in fair agreement with the literature values of 4.55 eV for W and 3 eV for Tb²¹.

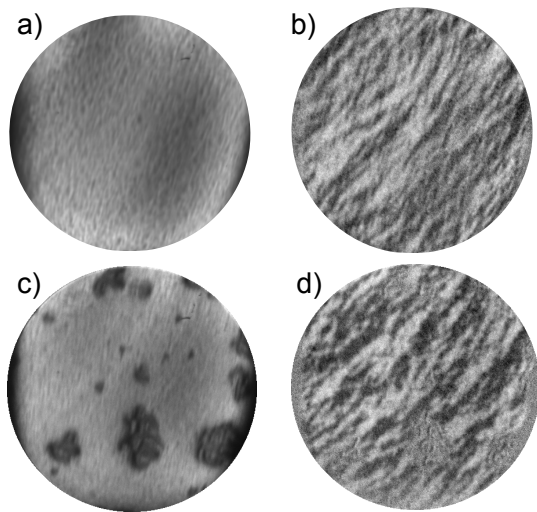


FIG. 3. (a) LEEM image showing the film topography after annealing at 650 K; (b) SPLEEM image with the electron polarization direction in-plane with azimuthal angle of 70° ; (c) LEEM and (d) SPLEEM images of a region containing holes due to dewetting of the substrate after annealing at 800 K, showing magnetic contrast only in the film region. The field of view is $12 \mu\text{m}$.

An image of the as-grown Tb films is shown in Fig. 1b. The step structure of the substrate is barely visible. In order to obtain lanthanide films with well-defined magnetic properties, it is important to achieve a good epitaxial morphology by choosing the appropriate annealing temperatures^{22,23}. Annealing the Tb films up to a temperature of 800 K leads to an increase of the reflected electron intensity (not shown) due to a smoothing of the film morphology. This is consistent with the significant reduction in the step density for annealing in the range of substrate temperatures of 600–800 K reported in Ref. [13]. In consequence, the Tb films were annealed up to a temperature of 650 K, and then cooled down to 80 K and analyzed by SPLEEM.

Figure 3a shows an annealed 20 ML Tb film at low temperature. This film is expected to be thick enough to possess essentially bulk-like magnetic properties. For example, epitaxial films of Fe^{24} or Co^{25} of 5 ML thickness already show the Curie temperatures of the bulk materials. For certain electron energies and using an in-plane spin polarization direction of the electron beam, magnetic contrast is detected in the normalized pixel-by-pixel difference image of LEEM images acquired with opposite spin-polarizations, shown in Fig. 3b. Black and white areas indicate regions where the magnetization has a non-zero component either parallel or antiparallel to the electron spin direction. The domain structure is ragged with domain walls that tend to follow the directions of the substrate steps, with typical widths of a few hundred nm. No component of the magnetization was detected in the out-of-plane direction.

To determine the orientation of the magnetization on the Tb film, pairs of SPLEEM images were acquired with the electron beam spin polarization aligned in orthogonal directions. Pixel intensity in the individual images represents Cartesian

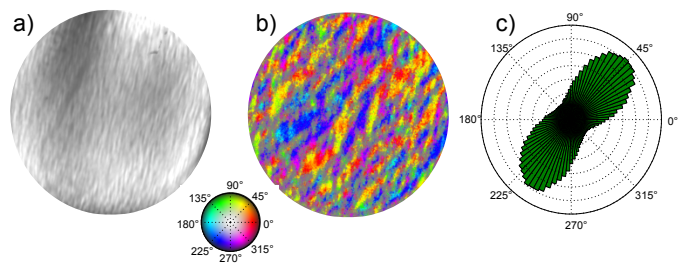


FIG. 4. (color online) (a) LEEM image showing the film topography after annealing at 650 K; (b) Composite color image combining SPLEEM images acquired with the spin-polarization of the electron beam at 87 and -3 deg. in-plane. (c) Polar histogram of magnetization directions in the area imaged in (b). Field of view is $12 \mu\text{m}$.

components of the magnetization vector, so that the 2D magnetization vector can be mapped. For the 20 ML Tb film shown in the LEEM image of Fig. 4a, this has been represented in Fig. 4b, where the magnetization orientation is given by the color according to the colormap shown below. To better visualize the angular distribution of the magnetization, a polar histogram²⁶ is shown in Fig. 4c. The histogram shown is based on an average of several pairs of images of the same region to improve the signal-to-noise ratio. The observed magnetization follows a broad uniaxial distribution with an axis of maximum contrast lying roughly at $45 \pm 20^\circ$. This can be related to the crystallographic orientation of the sample. Tb/W(110) films grow in the Nishiyama-Wassermann epitaxial relation¹³, i.e., with $\text{Tb}[11\bar{2}0]$ parallel to $\text{W}[001]$. The LEED patterns of our Tb films (not shown) indicate that $\text{Tb}[1\bar{1}00]$, which is parallel to $\text{W}[1\bar{1}0]$, lies at 25° in the angular coordinates of Fig. 4. The observed preferred direction of spontaneous magnetization lies close to a $\text{Tb}(0001)$ b -axis, the easy axis of bulk Tb metal⁸, in agreement with previous findings for epitaxial unmagnetized¹³ and remanently-magnetized Tb films²⁷. Nevertheless, other factors may introduce additional sources of anisotropy, such as the step distribution on the surface. The magnetic contrast in the images is produced by magnetic domains that extend preferentially along the main direction of the steps found in the substrate. Furthermore, the size of the domains visible in the images reaches several micrometers along the preferential step orientation. This is in contrast with the high-resolution images recorded by spin-polarized scanning tunneling microscopy (SPSTM) of Dy films on $\text{W}(110)$ ⁹, a system expected to be comparable to $\text{Tb}/\text{W}(110)$. There, much smaller domains, with sizes between 40 and 800 nm, can be observed. Domains seen with SPLEEM in our work might therefore represent an average of smaller domains with different orientations.

We have explored the dependence of the spin-asymmetry reflectivity on electron energy for a 20 ML Tb film. For this purpose, we measured SPLEEM images for different electron energies between 0 and 20 eV, and extracted the white-to-black contrast in the images. The results are shown in Fig. 5. The inserted images show an inverted contrast whenever the asymmetry curve changes sign (the apparent decrease of the magnetic contrast with increasing energy is due to the wors-

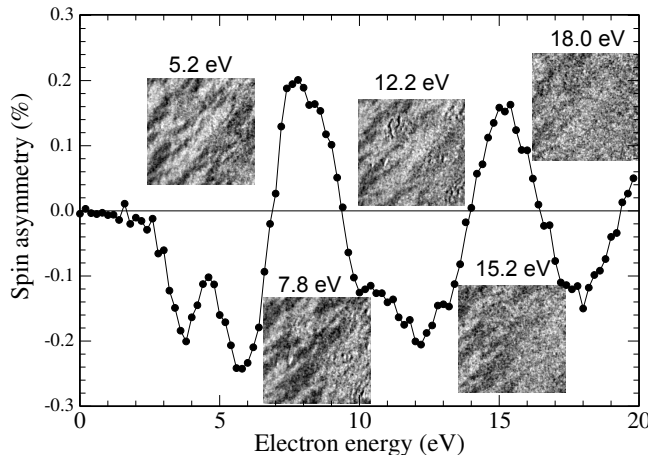


FIG. 5. Spin asymmetry of a 20 ML terbium film as a function of electron energy along the 47° direction. The images correspond to the energies indicated on top of each one and have a size of $3.9 \mu\text{m}$.

ening of the signal-to-noise ratio as a result of the decreasing net reflectivity, as shown by the inset of Fig. 2.) The asymmetry was measured along the 47° direction. The maximum of the asymmetry is around 0.2%, which, for a degree of spin polarization of the electron beam of about 20%, corresponds to a real asymmetry of the order of 1%. We can compare this value to the up to 10% asymmetry measured in 3d-transition metals²⁸, or the 16% asymmetry of magnetite²⁹. The experimental electron reflectivity has been compared in the past with theoretical calculations³⁰. However, we are unaware of such calculations in spin-split systems. The electronic states relevant for LEEM reflectivity are empty ones several eV's above the Fermi level. Spin asymmetry arises as a result of a difference in the density of states (DOS) for electrons of different spin orientations. This in turn depends on band splitting.

Spin-dependent reflectivity of a ferromagnetic surface is a result of two possible effects of the incoming spin-polarized beam scattering on the electrons of the target in their spin-split electronic states¹¹. The first one is the spin dependence of the elastic scattering potential and the second is inelastic electron-electron collisions with the result of scattering into unoccupied states, whose density of states (DOS) is different for both spin orientations. Since the inelastic mechanism leads to a reflectivity always higher for minority electrons¹¹, the oscillatory character of the spin asymmetry shown in Fig. 5 points to the presence of elastic scattering. Furthermore, the reduced asymmetry detected in terbium films is probably caused by the low spin polarization of the empty DOS induced by the localized $4f$ states of lanthanide metals, all of which appear at lower energies. In fact, experimental and theoretical results on the band structure of ferromagnetic Tb metal have shown an exchange splitting in the valence bands of about 1 eV ²⁷. This can be compared with the cases of Fe, with a band splitting of about 2 eV ³¹ and magnetite with a difference of the order of 3 eV between corresponding states for spin-up and spin-down electrons³².

Annealing over 800 K leads to increased step bunching and

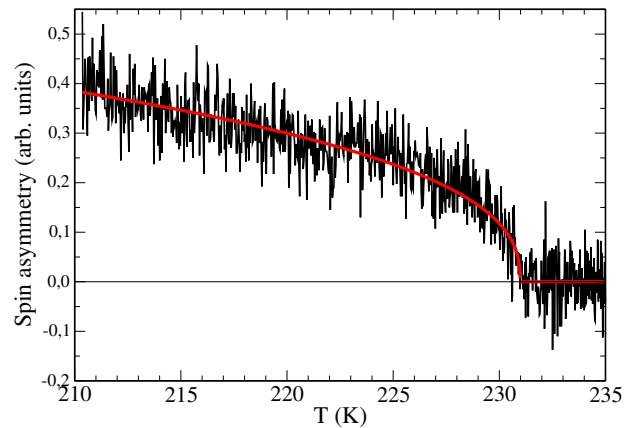


FIG. 6. (color online) Plot of the spin asymmetry, proportional to the sample magnetization, as a function of the temperature for a 20 ML Tb film at an electron energy of 2.9 eV along the 47° direction. The red line is a fit to an expression proportional to $(T_C - T)^\beta$, giving $\beta = 0.39$.

eventually the film breaks up by opening pinholes (see Fig. 3c) that extend down to the first Tb layer¹³, as observed for other metal films such as Cr on W(110)³³. Unlike Cr(110) films where the holes are strongly anisotropic, Tb(0001) pin-holes are more isotropic due to the hexagonal symmetry of the film's atomic lattice. This behavior correlates with the onset of a decrease of the Curie temperature of the Tb/W(110) films revealed by measurements of magnetic susceptibility in Ref. [13]. Figure 3d shows that magnetic contrast is observed in the Tb smooth areas but not in the pinholes. The bottom of the holes has been proposed to be covered by a single Tb monolayer, as shown by the LEED pattern observed after annealing to these temperatures¹³ and in accordance with the behavior of different rare-earth films on W(110) at monolayer and submonolayer coverages³⁴. Our result shows that the ordering temperature of this Tb monolayer lies below 80 K.

The evolution of the magnetic domains was followed upon raising the temperature and crossing the transition from the ferromagnetic to the helical antiferromagnetic phase. The distribution and shape of the domains does not change at all with temperature, suggesting that the domains are pinned down to structural defects. In fact, magnetic domains have been observed to be closely linked to the film morphology in the Dy/W system⁹. However, the magnetic contrast itself, measured by the spin-asymmetry in the reflectivity at a constant electron energy, changes with temperature. The magnetic contrast decreases upon increasing the temperature, disappearing at a temperature of 231 K, as shown in Fig. 6 for a 20 ML Tb/W(110) film. The magnetic contrast in SPLEEM can be considered a proxy of the magnetization. Thus the plot in Fig. 6 corresponds to the evolution of the magnetization with temperature. We note that the transition from the ferromagnetic to the helical antiferromagnetic phase is a first-order transition, while the transition from helical to paramagnetic is a conventional second-order magnetic-ordering transition. While SPLEEM is highly surface sensitive, for electron energies only a few eV's above the Fermi level, it actually probes

several atomic layers¹⁰, so the helical antiferromagnetic order is not expected to provide a significant contrast in SPLEEM. We thus assume that the disappearance of the magnetic contrast at the measured temperature of 231 K corresponds to the Curie temperature T_C of the film. This is in reasonable agreement with measurements by magnetic susceptibility on annealed Tb films¹³, where a similar value of the T_C of films annealed to these temperatures is observed.

A fit to an expression $M \sim (T_C - T)^\beta$ in Fig. 6 gives an exponent $\beta = 0.39 \pm 0.02$. This value is in remarkable coincidence with those found for other lanthanide metals, including systems with low (Gd, Ref[35]) and high (Ho, Ref[36]) values of the magnetocrystalline anisotropy. This confirms the bulk-like critical behaviour of our 20 ML thick films. Compared with the values of the critical exponent β for the three-dimensional (3D) models of Ising (0.326), X-Y (0.34), Heisenberg (0.365) and mean field (0.5), the value of 0.39 found in lanthanides has been interpreted for Gd in favour of a basically Heisenberg-like critical behaviour with dipolar contributions³⁷.

IV. SUMMARY

The magnetic domain structure of terbium films grown on W(110) was observed by SPLEEM. The polarization of the unoccupied density of states by the localized $4f$ levels gives rise to a spin-asymmetry reflectivity that was measured as a function of electron energy and reaches a maximum value of the order of 1%. The local orientation of the magnetization was detected by combining SPLEEM information along different angles. The ferromagnetic to helical antiferromagnetic transition was followed in real space while raising the temperature. While the domain distribution does not change through the transition, the magnetic contrast and thus the magnetization follows a critical exponent of 0.39, similar to the critical exponent measured by averaging techniques in different lanthanide metals such as Gd and Ho.

ACKNOWLEDGMENTS

This research was partly supported by Spain under Projects No. MAT2014-52477-C5-5-P, MAT2015-64110-C02-1-P (MINECO) and FIS2008-01431 (MICINN). Experiments were performed at the National Center for Electron Microscopy, Lawrence Berkeley National Laboratory, supported by the Office of Science, Office of Basic Energy Sciences, Scientific User Facilities Division, of the U.S. Department of Energy under Contract No. DE-AC02-05CH11231.

* joseemilio.prieto@uam.es

¹ W. Rodewald, in *Handbook of Magnetism and Advanced Magnetic Materials* (John Wiley & Sons, Ltd, 2007).
² D. Mergel, H. Heitmann, and P. Hansen, *Phys. Rev. B* **47**, 882 (1993).
³ J. F. Herbst, *Rev. Mod. Phys.* **63**, 819 (1991).
⁴ K. H. J. Buschow, *Rep. Prog. Phys.* **54**, 1123 (1991).
⁵ B. N. Harmon and A. J. Freeman, *Phys. Rev. B* **10**, 1979 (1974).
⁶ L. W. Roeland, G. J. Cock, F. A. Muller, A. C. Moleman, K. A. McEwen, R. G. Jordan, and D. W. Jones, *J. Phys. F* **5**, L233 (1975).
⁷ J. J. Rhyne and A. E. Clark, *J. App. Phys.* **38**, 1379 (1967).
⁸ J. J. Rhyne, in *Magnetic Properties of Rare Earth Metals*, edited by R. J. Elliott (Springer US, 1972) pp. 129–185.
⁹ L. Berbil-Bautista, S. Krause, M. Bode, and R. Wiesendanger, *Phys. Rev. B* **76**, 064411 (2007).
¹⁰ E. Bauer, *Surface Microscopy with Low Energy Electrons* (Springer Berlin Heidelberg, 2014).
¹¹ N. Rougemaille and A. K. Schmid, *Eur. Phys. J. Appl. Phys.* **50**, 20101 (2010).
¹² K. Starke, *Magnetic Dichroism in Core-Level Photoemission*, Springer Tracts in Modern Physics, Vol. 159 (Springer Berlin Heidelberg, Berlin, Heidelberg, 2000).
¹³ F. Heigl, J. E. Prieto, O. Krupin, K. Starke, G. Kaindl, and M. Bode, *Phys. Rev. B* **72**, 035417 (2005).
¹⁴ N. Rougemaille and A. K. Schmid, *J. App. Phys.* **99**, 08S502 (2006).

¹⁵ R. Ramchal, A. K. Schmid, M. Farle, and H. Poppa, *Phys. Rev. B* **69** (2004).
¹⁶ K. Grzelakowski, T. Duden, E. Bauer, H. Poppa, and S. Chiang, *IEEE Trans. Mag.* **30**, 4500 (1994).
¹⁷ T. Duden and E. Bauer, *Rev. Sci. Inst.* **66**, 2861 (1995).
¹⁸ F. El Gabaly, S. Gallego, C. Muñoz, L. Szunyogh, P. Weinberger, C. Klein, A. Schmid, K. McCarty, and J. de la Figuera, *Phys. Rev. Lett.* **96**, 147202 (2006).
¹⁹ M. Seah and W. Dench, *Surf. Interface Anal.* **1**, 2 (1979).
²⁰ L. Davis, N. MacDonald, P. Palmberg, G. Riach, and R. Weber, *Handbook of Auger Electron Spectroscopy* (Physical Electronics Division, Eden Prairie, Minnesota, 1978).
²¹ J. A. Dean, *Lange's Handbook of Chemistry, 15th. ed.* (McGraw-Hill, Inc., New York, 1999).
²² A. Aspelmeier, F. Gerhardt, and K. Baberschke, *J. Magn. Magn. Mat.* **132**, 22 (1994).
²³ K. Starke, L. Baumgarten, E. Arenholz, E. Navas, and G. Kaindl, *Physical Review B* **50**, 1317 (1994).
²⁴ M. Stambanoni, A. Vaterlaus, M. Aeschlimann, and F. Meier, *Phys. Rev. Lett.* **59**, 2483 (1987).
²⁵ C. M. Schneider, P. Bressler, P. Schuster, J. Kirschner, J. J. de Miguel, and R. Miranda, *Phys. Rev. Lett.* **64**, 1059 (1990).
²⁶ L. Martín-García, A. Mascaraque, B. M. Pabn, R. Bliem, G. S. Parkinson, G. Chen, A. K. Schmid, and J. de la Figuera, *Phys. Rev. B* **93**, 134419 (2016).
²⁷ K. M. Döbrich, G. Bihlmayer, K. Starke, J. E. Prieto, K. Rossnagel, H. Koh, E. Rotenberg, S. Blügel, and G. Kaindl, *Phys. Rev. B* **76**, 035123 (2007).

- ²⁸ J. Graf, C. Jozwiak, A. K. Schmid, Z. Hussain, and A. Lanzara, *Phys. Rev. B* **71**, 144429 (2005).
- ²⁹ J. de la Figuera, L. Vergara, A. T. N'Diaye, A. Quesada, and A. K. Schmid, *Ultramicroscopy* **130**, 77 (2013).
- ³⁰ J. I. Flege and E. E. Krasovskii, *Phys. Status Solidi RRL* **8**, 463 (2014).
- ³¹ A. Santoni and F. J. Himpsel, *Phys. Rev. B* **43**, 1305 (1991).
- ³² M. Fonin, Y. S. Dedkov, R. Pentcheva, U. Rüdiger, and G. Güntherodt, *J. Phys.: Condens. Matter* **19**, 315217 (2007).
- ³³ K. McCarty, J. Hamilton, Y. Sato, A. Saa, R. Stumpf, J. de la Figuera, K. Thurmer, F. Jones, A. Schmid, A. Talin, and N. Bartelt, *New J. Phys.* **11**, 043001 (2009).
- ³⁴ J. Kołaczkiwicz and E. Bauer, *Surface Science* **175**, 487 (1986).
- ³⁵ A. G. A. M. Saleh and N. H. Saunders, *J. Magn. Magn. Mat.* **29**, 197 (1982).
- ³⁶ J. Eckert and G. Shirane, *Solid State Comm.* **19**, 911 (1976).
- ³⁷ E. Frey, F. Schwabl, S. Henneberger, O. Hartmann, R. W. Wäppling, A. Kratzer, and G. E. Kalvius, *Phys. Rev. Lett.* **79**, 5142 (1997).